Euler Solutions Simulating Strong Shock Waves and Vortex Phenomena over 3D Wings

Fan Meng and Ma Tieyou
Beijing University of Aeronautics and Astronautics
Beijing, China

Abstract

Based on Beam & Warming's Implicit Approximate Factorization Algorithm this paper solves conservative Euler equations on arbitrary curvilineal coordinates. The algorithm with diagonal form and local time step is used to obtain a faster convergence rate. The ONERA M6 Wing's C-H grid is generated by using an algebraic method. Results in strong shock case are obtained. By comparing the computed results with experimental data, the feasility of the algorithm has been tested and verified. This paper still used C-H grid to simulate the leading edge and wing tip vortex flow phenomena over delta wing at subsonic Mach numbers. A hybrid method in diagonal form has been tested for accelerating convergence rate, which saves about 11% CPU time for each step.

Introduction

Accurate and cost-effective simulation of three dimensional flows dominated by free vortex or when strong shock waves develop, which are typical in the flight of fighter aircraft, continues to be one of the challenging problems. The leading-edge separated vortices are the subject of the present investigation. They form on the leeward side of swept slender wings at moderate to high angles of attack during low-speed flight or transonic maneuvering. Considerable improvement in aerodynamic performance can be obtained by careful generation and control of these vortices. Accurate, efficient and reliable computational methods are needed to properly simulate such flowfields.

The main emphasis in this paper has been placed on applicability of the method and on achieving accuracy. We make some effort mentioned in following towards achieving a fast algorithm. We make some effort mentioned in following towards achieving a fast algorithm. The first application is the simulation of the flowfield over AGARD ONERA M6 Wing in strong shock case. The second application is that of the leading-edge separation vortex over a delta wing at moderate to high angles of attack. These results indicate that the present approach is capable of computing complicated three-dimensional flow fields.

Governing Equations and Numerical Algorithm

Governing Equations

The basic equations under consideration here are the unsteady Euler equations. These are specialized to a body fitted coordinate system (ξ,η,ζ) where the ξ-coordinate lines are along streamwise direction and the ζ-coordinate lines are nearly orthogonal to the body surface. The governing equations for a coordinate system fixed in time can then be written in nondimensional conservation-law form as follows:

$$\frac{\partial \hat{U}}{\partial t}+\frac{\partial \hat{E}}{\partial \xi}+\frac{\partial \hat{F}}{\partial \eta}+\frac{\partial \hat{G}}{\partial \zeta}=0 \tag{1}$$

where

$$\hat{U}=J^{-1}\begin{bmatrix}\rho\\ \rho u\\ \rho v\\ \rho w\\ e\end{bmatrix} \qquad \hat{E}=J^{-1}\begin{bmatrix}\rho U\\ \rho uU+\xi_x p\\ \rho vU+\xi_y p\\ \rho wU+\xi_z p\\ (e+p)U\end{bmatrix} \tag{2}$$

$$\hat{F}=J^{-1}\begin{bmatrix}\rho V\\ \rho uV+\eta_x p\\ \rho vV+\eta_y p\\ \rho wV+\eta_z p\\ (e+p)V\end{bmatrix} \qquad \hat{G}=\begin{bmatrix}\rho W\\ \rho uW+\zeta_x p\\ \rho vW+\zeta_y p\\ \rho wW+\zeta_z p\\ (e+p)W\end{bmatrix}$$

The contravariant velocity components are defined as

$$\begin{bmatrix}U\\ V\\ W\end{bmatrix}=\begin{bmatrix}\xi_x u+\xi_y v+\xi_z w\\ \eta_x u+\eta_y v+\eta_z w\\ \zeta_x u+\zeta_y v+\zeta_z w\end{bmatrix} \tag{3}$$

The transformation metrics are defined as follows:

$$\begin{vmatrix}\xi_x & \xi_y & \xi_z\\ \eta_x & \eta_y & \eta_z\\ \zeta_x & \zeta_y & \zeta_z\end{vmatrix}= =J\begin{vmatrix}(y_\eta z_\zeta-y_\zeta z_\eta) & (z_\eta x_\zeta-x_\eta z_\zeta) & (x_\eta y_\zeta-y_\eta x_\zeta)\\ (z_\xi y_\zeta-y_\xi z_\zeta) & (x_\xi z_\zeta-x_\zeta z_\xi) & (y_\xi x_\zeta-x_\xi y_\zeta)\\ (y_\xi z_\eta-z_\xi y_\eta) & (x_\eta z_\xi-x_\xi z_\eta) & (x_\xi y_\eta-y_\xi x_\eta)\end{vmatrix} \tag{4}$$

where J is the Jacobian of transformation given by

$$J^{-1}=x_\xi(y_\eta z_\zeta-y_\zeta z_\eta)-y_\xi(x_\eta z_\zeta-x_\zeta z_\eta)+z_\xi(x_\eta y_\zeta-y_\eta x_\zeta) \tag{5}$$

The pressure is related to the other flow variables for an ideal gas by the following equation of state

$$p=(\gamma-1)[e-0.5\rho(u^2+v^2+w^2)] \tag{6}$$

Numerical Algorithm

Starting with the implicit approximate factorization scheme developed by Beam and Warming [1]

$$(I+h\frac{\partial\hat{A}^n}{\partial\xi})(I+h\frac{\partial\hat{B}^n}{\partial\eta})(I+h\frac{\partial\hat{C}^n}{\partial\zeta})(\hat{U}^{n+1}-\hat{U}^n)=RHS \tag{7}$$

$$RHS=-\Delta t(\frac{\partial\hat{E}^n}{\partial\xi}+\frac{\partial\hat{F}^n}{\partial\eta}+\frac{\partial\hat{G}^n}{\partial\zeta}) \tag{8}$$

where $\hat{A}$, $\hat{B}$ and $\hat{C}$ are the Jacobian matrices $\partial\hat{E}/\partial\hat{U}$, $\partial\hat{F}/\partial\hat{U}$ and $\partial\hat{G}/\partial\hat{U}$

The flux Jacobians $\hat{A}$, $\hat{B}$ and $\hat{C}$ each have real eigenvalues and a complete set of eigenvectors. Therefore the Jacobian matrices can be diagonalized.

$$\Lambda_\xi=T_\xi^{-1}\hat{A}T_\xi=$$
$$=Dig(U,U,U,U+a\sqrt{\xi_x^2+\xi_y^2+\xi_z^2},$$
$$U-a\sqrt{\xi_x^2+\xi_y^2+\xi_z^2})$$
$$\Lambda_\eta=T_\eta^{-1}\hat{B}T_\eta=$$
$$=Dig(V,V,V,V+a\sqrt{\eta_x^2+\eta_y^2+\eta_z^2},$$
$$V-a\sqrt{\eta_x^2+\eta_y^2+\eta_z^2})$$
$$\Lambda_\zeta=T_\zeta^{-1}\hat{C}T_\zeta=$$
$$=Dig(W,W,W,W+a\sqrt{\zeta_x^2+\zeta_y^2+\zeta_z^2},$$
$$W-a\sqrt{\zeta_x^2+\zeta_y^2+\zeta_z^2}) \tag{9}$$

Then AF scheme in diagonal form can be written as [2]:

$$T_\xi[I+h\frac{\partial\Lambda_\xi}{\partial\xi}]\hat{N}[I+h\frac{\partial\Lambda_\eta}{\partial\eta}]\hat{M}[I+h\frac{\partial\Lambda_\zeta}{\partial\zeta}]T_\zeta^{-1}\cdot\Delta\hat{U}=RHS \tag{10}$$

where $\hat{N}=T_\xi^{-1}T_\eta$, $\hat{M}=T_\eta^{-1}T_\zeta$

Compared to using full block algorithm there are significant advantages to the diagonal algorithm. First it reduced the computational work and the second it requires less temporary storage than the block algorithm.

We solve the above equations (10) in following steps:

$$[\hat{\mu}_i+h\hat{\delta}_i\Lambda_\xi-D_i/_\xi]\Delta\hat{U}_{ijk}^{**}=T_\xi^{-1}(RHS-D_e)$$
$$[I+h\delta_j\Lambda_\eta-D_i/_\eta]\Delta\hat{U}_{ijk}^{**}=\hat{N}^{-1}\Delta\hat{U}_{ijk}^{**}$$
$$[I+h\delta_k\Lambda_\zeta-D_i/_\zeta]\Delta\hat{U}_{ijk}^{*}=\hat{M}^{-1}\Delta\hat{U}_{ijk}^{**} \tag{11}$$
$$\Delta\hat{U}_{ijk}=T_\zeta\Delta\hat{U}_{ijk}^{*}$$
$$\hat{U}_{ijk}^{n+1}=\hat{U}_{ijk}^{n}+\Delta\hat{U}_{ijk}$$

where

$$RHS=-\Delta t[\hat{\delta}_i\hat{E}+\hat{\mu}_i\delta_j\hat{F}+\hat{\mu}_i\delta_k\hat{G}]$$
$$D_i/_\xi=\varepsilon_i\Delta tJ^{-1}(\nabla_\xi\Delta_\xi)J$$
$$D_i/_\eta=\varepsilon_i\Delta tJ^{-1}(\nabla_\eta\Delta_\eta)J$$
$$D_i/_\zeta=\varepsilon_i\Delta tJ^{-1}(\nabla_\zeta\Delta_\zeta)J \tag{12}$$
$$D_e=\varepsilon_E\Delta tJ^{-1}[(\nabla_\xi-\varepsilon_i\nabla_\xi)\Delta_\xi\nabla_\xi\Delta_\xi+(\nabla_\eta\Delta_\eta)^2+$$
$$+(\nabla_\zeta\Delta_\zeta)^2]J\hat{U}$$

where δ is the central difference operator, and Δ and ∇ are forward and backward difference operators, respectively. D_i represent implicit second-order smoothing terms. D_e represents explicit fouth-order smoothing terms.

Central differencing is used throughout the solution domain, except in the region of supersonic flow before a shock. Upwind differencing before shocks has a stabilizing effect and improves the accuracy of the calculations. Here we use a combined operator which has a free parameter ε_i such that $\varepsilon_i=0$ produces the central operator and $\varepsilon_i=1$ gives the one-sided operator. The difference scheme in the following manner is conservative [3]

$$\tilde{\delta}_i=\frac{I-\nabla_\xi\varepsilon_i}{\frac{1}{2}(2I-\varepsilon_iI+E^-\varepsilon_i)}\delta_i \tag{13}$$

where $E^-u_i=u_{i-1}$

Rewriting the above Eq. (13) as

$$\tilde{\delta}_i=\hat{\delta}_i/\hat{\mu}_i$$

where $\hat{\delta}_i=(I-\nabla_\xi\varepsilon_i)\delta_i$ $\qquad\hat{\mu}_i=\frac{1}{2}(2I-\varepsilon_iI+E^-\varepsilon_i)$

Mesh Generation and Boundary Conditions

Mesh Generation

A body conforming C-H mesh is generated about an arbitrary wing using an algebraic method.

At first the position of each C-like computational mesh in the chordwise section should be given in the spanwise direction.

The C-like computational mesh is founded on the curvilineal coordinate system ξ,ζ, for which the line $\zeta=\zeta_{min}$ coincides with the airfoil. One family of hyperbolas of coordinate curves that should intersect the airfoil (ξ is constant) is adopted, given in the parameter θ by

$$x=B+A\cosh(\zeta)\cos\theta$$
$$z=A\sinh(\zeta)\sin\theta \tag{14}$$

The origins of the hyperbolas ξ_i, ζ_{min} are set by the desired distribution of points on the airfoil. The farfield boundary is defined as an ellipse:

$$\frac{(x-B)^2}{x_{FAR}^2}+\frac{z^2}{z_{FAR}^2}=1 \tag{15}$$

At the leading and trailing edges the first mesh interval in the ξ direction is specified and the remaining are then calculated from the spline fit interpolation according to the arclength distribution. Also the first mesh interval in the ζ direction in the leading and trailing edges is specified and the remaining are then calculated from a quadratic relation between these two. Subsequent intervals are prescribed by an exponential stretching function. That part of the mesh past the trailing edge is obtained by translating the hyperbola at the trailing edge downstream to the last desired position.

Boundary Conditions

At the body surface, tangence is satisfied by $V_n=0$. The tangential velocity U_1, V_1 are obtained at the body surface through linear extrapolation. The cartesian velocities are then formed from the inverse relation

$$\begin{bmatrix}u\\v\\w\end{bmatrix}=$$

$$J^{-1}\begin{bmatrix}(\eta_y\zeta_z-\eta_z\zeta_y) & -(\xi_y\zeta_z-\xi_z\zeta_y) & (\eta_z\zeta_y-\eta_y\zeta_z)\\ (\eta_x\zeta_z-\eta_z\zeta_x) & (\xi_x\zeta_z-\xi_z\zeta_x) & -(\eta_z\zeta_x-\eta_x\zeta_z)\\ (\eta_x\zeta_y-\eta_y\zeta_x) & -(\xi_x\zeta_y-\xi_y\zeta_x) & (\eta_y\zeta_x-\eta_x\zeta_y)\end{bmatrix}\begin{bmatrix}U_1\\ V_1\\ 0\end{bmatrix} \tag{16}$$

The pressure on the body surface is obtained from the normal momentum equation

$$(\xi_x\zeta_x+\xi_y\zeta_y+\xi_z\zeta_z)p_\xi+(\eta_x\zeta_x+\eta_y\zeta_y+\eta_z\zeta_z)p_\eta+(\zeta_x^2+\zeta_y^2+\zeta_z^2)p_\zeta$$
$$=-\rho U(\zeta_x u_\xi+\zeta_y v_\xi+\zeta_z w_\xi)-\rho V(\zeta_x u_\eta+\zeta_y v_\eta+\zeta_z w_\eta) \tag{17}$$

Adiabatic walls are used to obtain density at the surface.

Far-field boundary conditions are given as far-field inflow conditions. At the outflow boundary, variables are all calculated from inside the computational domain except that pressure is specified as p_∞ at the subsonic outflow. Symmetry conditions are used at the root section for a finite wing.

Convergence Acceleration and Scheme Improvement

Convergence has been improved significantly by use of local maximum time step and by using a diagonal form of AF scheme.

Here we also adopt a hybrid method similar to which was developed by L. N. Sankar, etc[4]. For the eqs. (1), the spanwise derivative $\frac{\partial\hat{F}}{\partial\eta}$ was written as a combination of the n and n+1 time levels. During the odd time steps, calculations were done on span station at a time, from the wing root to the outboard span station, using the latest values of the flow vector at the (n+1) time level as soon as available. Thus

$$\partial\hat{F}/\partial\eta=(F^n_{j+1}-F^{n+1}_{j-1})/2 \tag{18a}$$

During the even time steps the calculations started at the last span station outboard and progressed until the root station was reached. Then the term

$$\partial\hat{F}/\partial\eta=(F^{n+1}_{j+1}-F^n_{j-1})/2 \tag{18b}$$

Removing the term $\partial\hat{F}/\partial\eta$ from lefthand side of the eqs. (1) to the right and adopting diagonal AF scheme results in the following equation:

$$T_\xi(\hat{\mu}_i+h\hat{\delta}_i\Lambda_\xi-D_i/_\xi)\hat{P}(I+h\delta_k\Lambda_\zeta-D_i/_\zeta)T_\zeta^{-1}\Delta U=$$
$$=-\Delta t[\hat{\delta}_i\hat{E}+\hat{\mu}_i\delta_k\hat{G}+\frac{\partial\hat{F}}{\partial\eta}]-D_e \tag{19}$$

Where $\hat{P}=T_\xi^{-1}T_\zeta$

The advantage of the hybrid scheme as above is that it requires less CPU time for each time step and also it requires less computer memory.

Results and Discussion

In this section, results are presented for two cases: strong shock flow over M6 wing, and vortex flow over a 56° cropped delta wing. For each case, the entire domain is initialized to freestream conditions. All calculations have been done on a super-microcomputer with 16MB Memory. The processing time required is approximately 0. 0019 secs/grid point/time step, and 1000 - 1500 iterations were necessary to obtain steady state solutions.

Strong Shock Flow over M6 Wing

As a standard test configuration having a great deal of experimental data avaiable[6], AGARD ONERA M6 wing (Fig. 1) is usually used as a typical example to evaluate computer code. The M6 wing's C-H grid (151×20×20) is shown in Fig. 2. Computed results for the strong shock case (M_∞ = 0. 84, α=3. 06°) are presented in Fig. 3 through Fig. 5. In this case appear the well known triple shock waves. The merging of the two shocks into one toward the wing tip forming a typical λ-type pattern is clearly evident in Fig. 4 and Fig. 5. The agreement with experiment is reasonably good at most span stations. (Fig. 3) The results of the computation on 103 ×16×20 mesh for this case exhibited poor agreement with test data. Only one strong shock was captured. It is anticipated that to resolve this flow field, a higher grid density is needed.

Free Vortex Flow over a 57° Cropped Delta Wing

The 57° cropped delta wing with a taper ratio of 0. 078, and an aspect ratio of 2. 223 is shown in Fig. 6. A comparison of the computed and measured aerodynamic parameters is shown in Fig. 7 for three angles of attack (8°, 16°, 24°) at a free stream of Mach number 0. 6. For these computations a 83 ×25×20 C-H mesh is used. The agreement between the computations and measurements is quite good. The corelations indicate that the computed results include the nonlinear part of the vortex lift. Computed results for the angles of attack of 24° are presented in Fig. 8 through Fig. 10. Fig. 8 shows the spanwise station plane velocity fields. The particle path traces are shown in Fig. 9. The leading edge vortex flow phenomena is very clear. The negative pressure distribution on the upper surface of the wing is shown in Fig. 10. The same computation also be made on a 65×20×15 mesh, it is found that grid refinement does not significantly alter the results. And also magnifying the numerical dissipation has no effect on the results.

Conclusion

Use of Euler codes appears to be an attractive alternative to using the Navier-Stokes codes that require greater computational resources. The Euler equations, which cannot describe flow separation mathematicaly as we know, appear to give reasonable results because flow separates at the leading edge owning to the numerical dissipations. The results above indicate that the present approach is capable of computing complicated three-dimensional flow fields.

References

1. Beam, R. M. and Warming, R. F., "An Implicit Factored Scheme for the Compressible Navier-Stokes Equations", AIAA J., Vol. 16, No. 4, 1978
2. Pulliam, T. H. and Chaussee, D. S., "A Diagonal Form of an Implicit Approximation -Factorization Algorithm", J. of Comput. Phys., Vol. 39, 1981, pp. 347-363
3. T. H. Pulliam, D. C. Jespersen and R. E. Childs, "An Enhanced Version of an Implicit Code for the Euler Equations", AIAA 83-0344
4. N. L. Sankar, J. B. Malone and D. Schuster, "Euler Solutions for Transonic Flow Past a Fighter Wing", J. Aircraft, 1987, Vol. 24, No. 1, pp. 10～16
5. Schmitt, V., and Charpin, F., "Pressure Distributions on the ONERA-M6-Wing at Transonic Mach Numbers", AGARD-AR-138, Chapter B-1, 1984
6. Thomas H. Pulliam and Joseph L. Steger, "Recent Improvements in Efficiency, Accuracy, and Convergence for Implicit Approximate Factorization Algorithms", AIAA 85-0360
7. P. Raj and J. S. Sikora, "Free-Vortex Flows; Recent Encounters with an Euler Code", AIAA 84-0135
8. K. Fujii, S. Gravali and T. L. Holst, "Evaluation of Navier-Stokes and Euler Solutions for Leading-Edge Separation Vortices", International Journal for Numerical Methods in Fluids, Vol. 8, 1988
9. P. Raj, J. S. Sikora and J. M. Keen, "Free-Vortex Flow Simulation Using a Three-Dimensional Euler Aerodynamic Method", J. Aircraft, Vol. 25, No. 2, 1988
10. Newsome, R. W. and Thomas J. "Computation of Leading-Edge Vortex Flow", NASA CP-2416, 1986
11. V. N. Vatsa, "Accurate Solutions for Transonic Viscous Flow Over Finite Wings", AIAA 86-1052

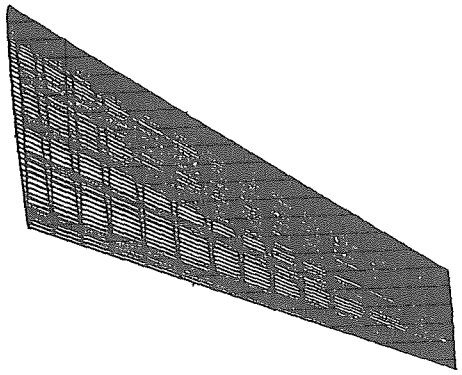

Fig. 1 AGAGD ONERA M6 Wing

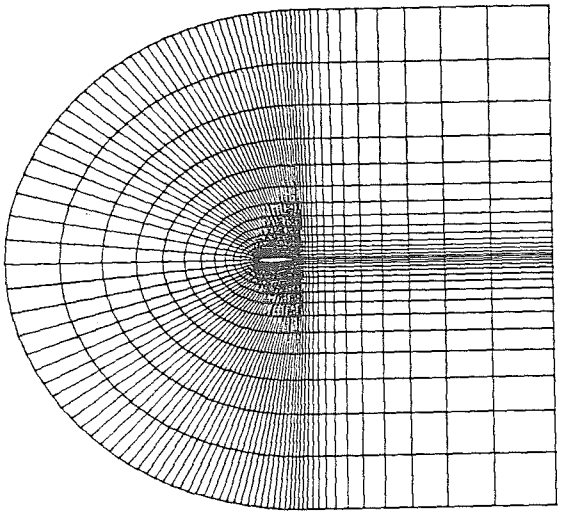

(a)C-like Computational Mesh in the Chordwise Direction

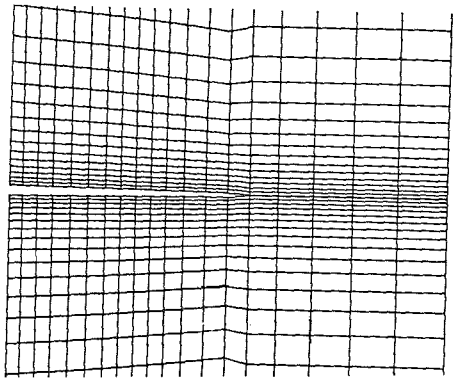

(b) H- like Computational Mesh in the Spanwise Direction

Fig. 2 C-H mesh

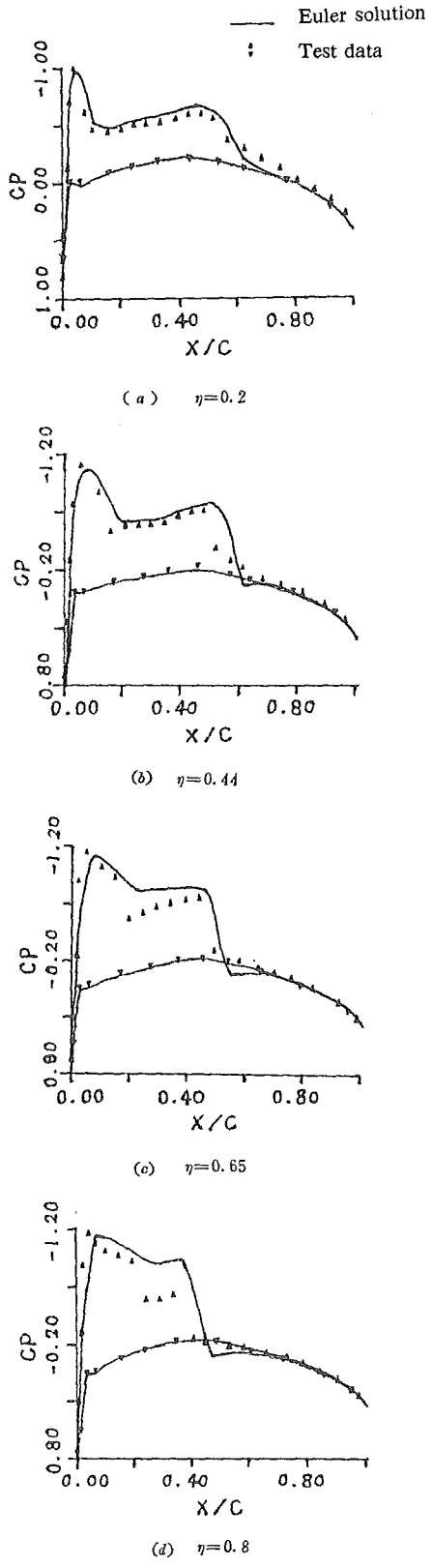

Fig. 3 Chordwise C_p Distribution on ONERA M6 Wing
$M_\infty = 0.84$, $\alpha = 3.06°$

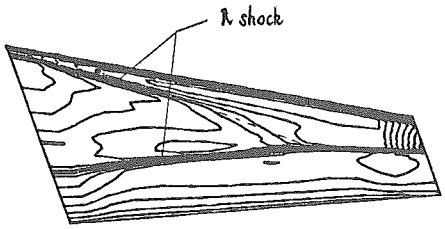

Fig. 4 Pressure Contours on Upper Surface of M6 Wing
$M_\infty = 0.84$, $\alpha = 3.06°$

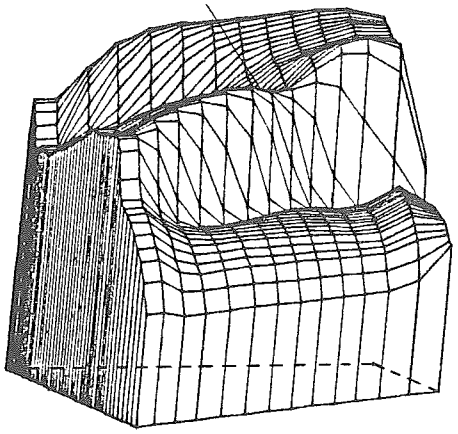

Fig. 5 Negative Pressure Distribution on Upper Surface of M6 Wing
$M_\infty = 0.84$ $\alpha = 3.06°$

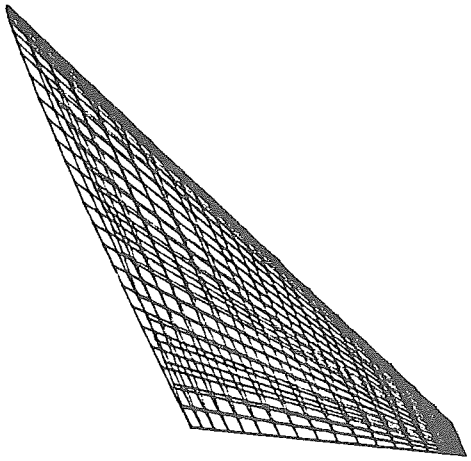

Fig. 6 57° Cropped Delta Wing

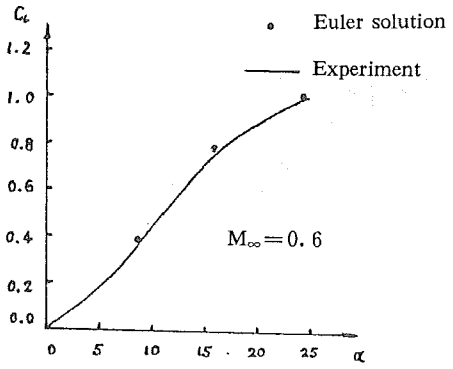

Fig. 7 Correlation of Computed Aerodynamic Parameters with Experimental Data for 57° Cropped Delta Wing

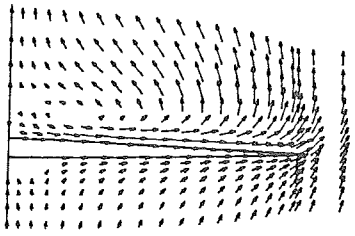

(a) I=32 station

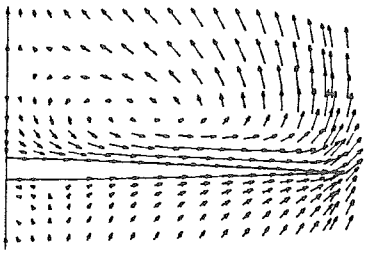

(b) I=28 station

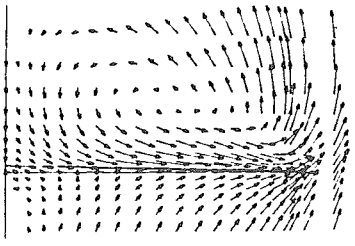

(c)I = 20 station

Fig. 8 Computed Spanwise Station Plane Velocity Fields
$M_\infty = 0.6$ $\alpha = 24°$

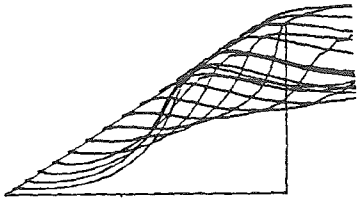

(a) Top View

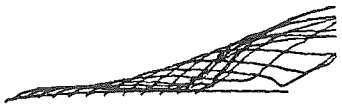

(b) Side View

Fig. 9 Particle Path Traces ($M_\infty = 0.6$, $\alpha = 24°$)

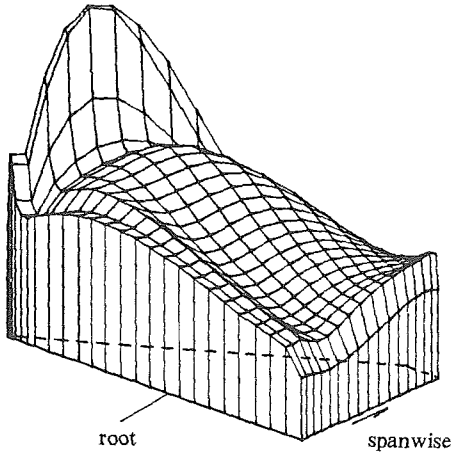

Fig. 10 Negative Pressure Distribution on Upper Surface of the Cropped Wing

$M_\infty = 0.6$ $\alpha = 24°$